

Supporting Information

Cubic Superstructures Composed of PtPd Alloy Nanocubes and their Enhanced Electrocatalysis for Methanol Oxidation

Lin-Nan Zhou,^a Xiao-Ting Zhang,^a Ze-Hong Wang,^a Shaojun Guo,^{b*} Yong-Jun Li^{a*}

^aState Key Lab of Chemo/Biosensing and Chemometrics, School of Chemistry and Chemical Engineering, Hunan University, Changsha 410082, China. E-mail: liyje@hnu.edu.cn

^bDepartment of Materials Science and Engineering, College of Engineering, Peking University, Beijing, P.R. China. E-mail: guosj@pku.edu.cn

Experimental Section

Chemicals. Hexachloroplatinic (IV) acid hexahydrate ($\text{H}_2\text{PtCl}_6 \cdot 6\text{H}_2\text{O}$, 99.9 %), palladium(II) chloride (PdCl_2 , 99.9 %), poly(vinylpyrrolidone) (PVP, $M_w \approx 29000$), KI (AR), and ethylene glycol (EG, AR) were purchased from Sinopharm Chemical Reagent Co., Ltd. All chemical reagents were used as received. Ultrapure Millipore water ($18.2 \text{ M}\Omega \cdot \text{cm}$) was used as the solvent throughout.

20 M H_2PdCl_4 stock solution was prepared by dissolving 0.356 g of PdCl_2 into 0.417 mL of 12 M HCl aqueous solution and diluted to 100 mL with water.

Growth of $\text{Pt}_{50}\text{Pd}_{50}$ nanocube superstructure. Typically, 0.5 mL of 20 mM H_2PdCl_4 stock solution and 0.5 mL of 20 mM H_2PtCl_6 aqueous solution were added into 20 mL EG containing PVP (160 mg). To the mixture was added 110 μL of 5 M KI aqueous solution and the solution color changed from brown to chestnut. Subsequently, the homogeneous mixture was heated to 150 °C in an oil bath, refluxed for 60 min with vigorous stirring, and naturally cooled to room temperature. The product was collected by centrifugation at 5 000 rpm, washed successively with acetone, ethanol and water. Finally, the clean product was redispersed into a certain amount of ethanol. By changing the H_2PtCl_6 : H_2PdCl_4 molar ratio, PtPd alloy particles with changeable compositions and morphologies can be obtained (Table S2).

Fabrication of catalytic electrode and electrochemical measurement. 2.5 mg of Vulcan C was added into 1.0 mL of PtPd particle ethanol solution (Table S3), and vigorously sonicated

to obtain PtPd/C catalyst ink. 3 mg Pt/C (20 wt%) was dispersed into 1 mL ethanol. A certain volume of PtPd/C or Pt/C suspension (Table S3) was applied to a glassy carbon disk (GCD, diameter, 3 mm) by a drop-coating method and dried at ambient condition, and subsequently 5 μ L of Nafion alcohol solution (0.05 wt%) was covered to solidify the catalyst layer. The final mass of each catalyst was fixed at \sim 5 μ g on GC surface.

All electrochemical measurements were carried out in a conventional three-electrode cell. A saturated calomel electrode (SCE) and a Pt sheet were used as the reference electrode and the counter electrode, respectively. GCDs loading catalysts are the working electrodes. Prior to catalyst deposition, GCD was polished successively with 1.0 μ m, 0.3 μ m and 0.05 μ m alumina powders and rinsed by sonication in deionized water.

Before electrocatalytic measurements, all catalytic electrodes were cleaned by cycling between -0.25 and 1.42 V at 50 $\text{mV}\cdot\text{s}^{-1}$ in 0.5 M H_2SO_4 solution until stable cycle voltammograms were obtained. Electrocatalytic performance of catalysts was evaluated by cyclic voltammetric and chronoamperimetric techniques in N_2 -saturated 1.0 M KOH solution containing 1.0 M CH_3OH .

Other characterizations and instruments. Electrochemical experiments were performed on a CHI 660D workstation (Chenhua, Shanghai). Transmission electron microscopy (TEM), high resolution transmission electron microscopy (HRTEM), and energy dispersive X-ray (EDX) spectra were obtained on a JEM-3010 microscope (JEOL, Japan). High angle annular dark field scanning-transmission electron microscopy (HAADF-STEM) and HAADF-STEM-EDX element line scans/mapping were performed on a Tecnai G2 F20 S-Twin high-resolution transmission electron microscope operating at 200 kV. Inductively coupled plasma optical emission spectrometry (ICP-OES) was performed on IRIS Intrepid II XSP (Thermo Fisher). X-ray diffraction (XRD) measurement was performed on a θ - 2θ X-ray diffraction Shimadzu XRD-6100.

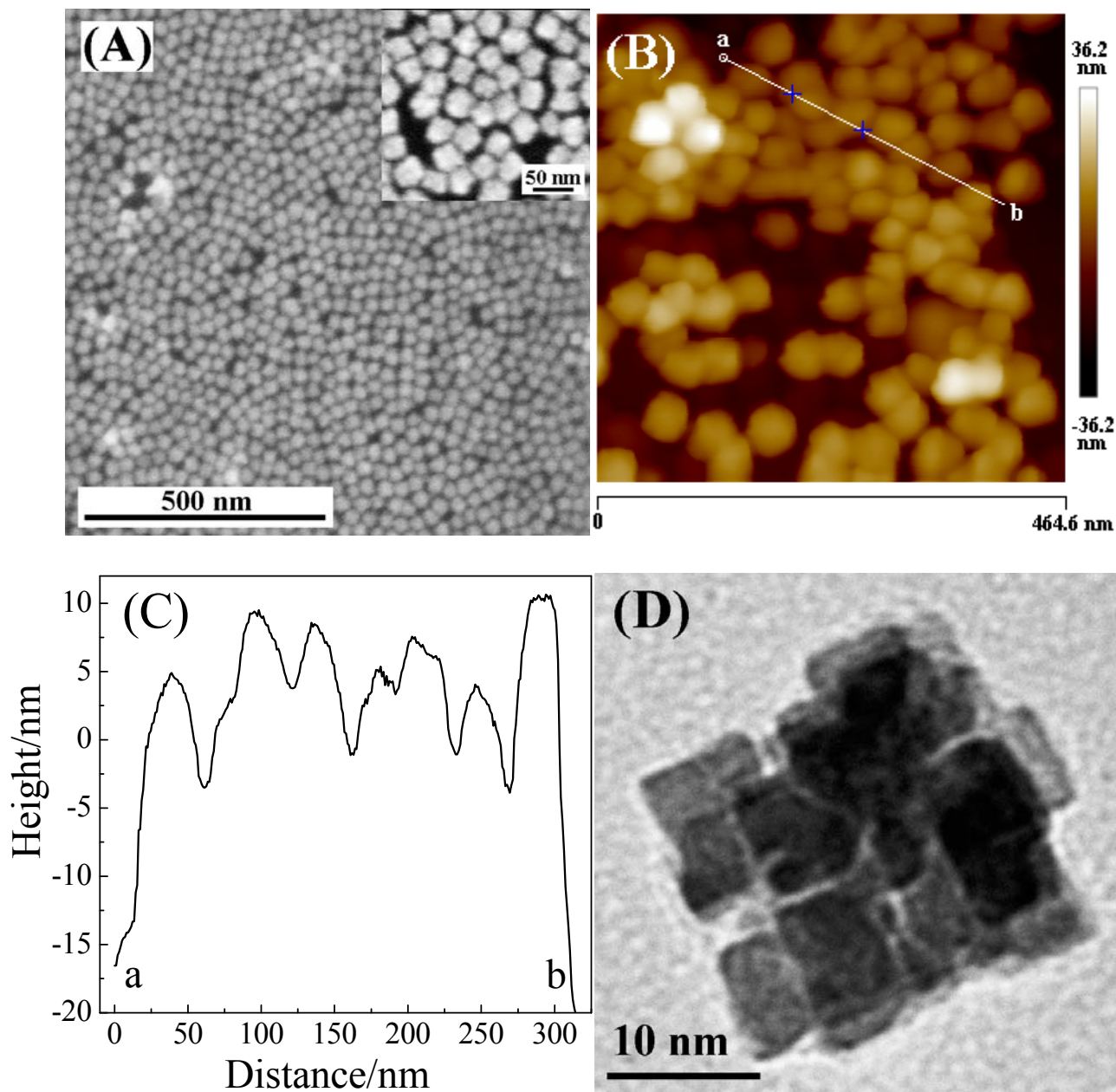


Fig. S1 SEM (A and the inset), AFM (B) and TEM (D) images of Pt₅₀Pd₅₀ CSs, and the height profile scanning from a to b marked in Fig. S1B (C). (AFM cannot really disclose the true morphology and the size of Pt₅₀Pd₅₀ CS because the resolution of AFM scan in a two-dimensional plane is extremely low due to the effect caused by the width of AFM tip¹. Thus, Pt₅₀Pd₅₀ CSs look like spheres in the topographic phase image (Fig. S1B), and the average diameter of ~41 nm is larger than the side length measured according to SEM and TEM images. However, the line scan profile can provide accurate information about the height because there is no the effect of the tip width¹.)

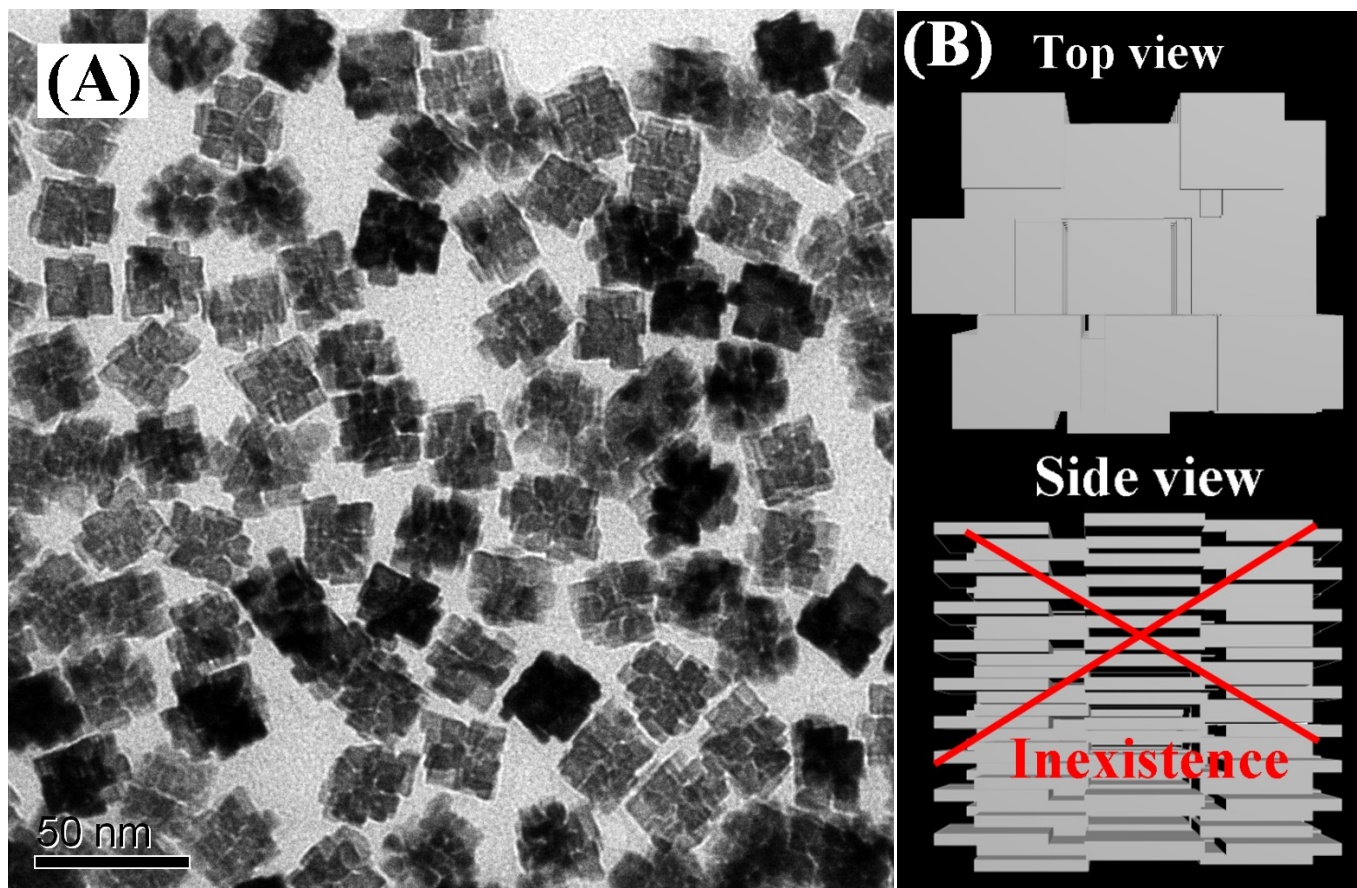


Fig. S2 (A) TEM image of Pt₅₀Pd₅₀ CSs. (B) Illustration of the top view and side view if Pt₅₀Pd₅₀ is composed of cubic nanosheets. Actually, Pt₅₀Pd₅₀ CSs are made up with nanocubes and the side view as illustrated does not exist.

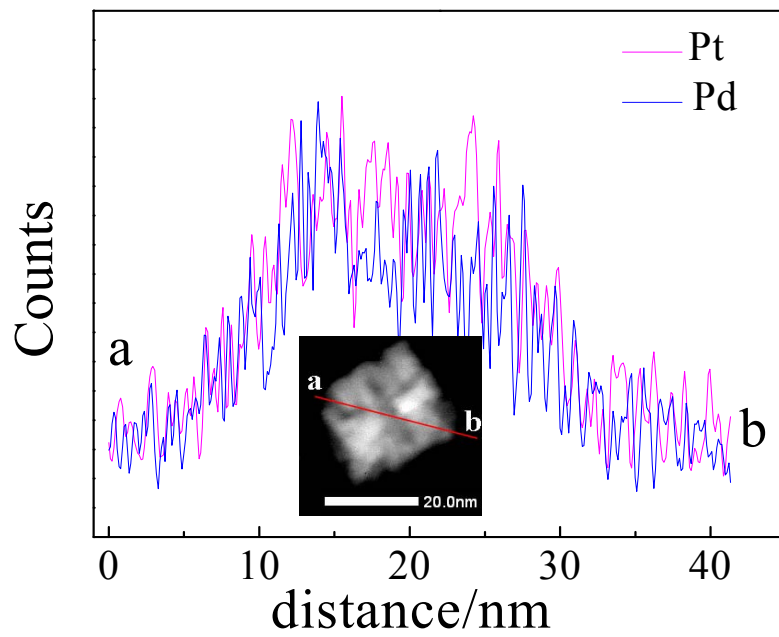
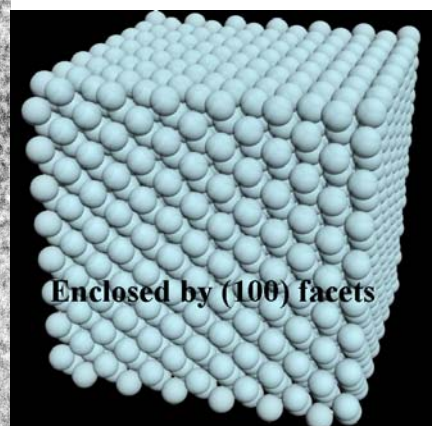
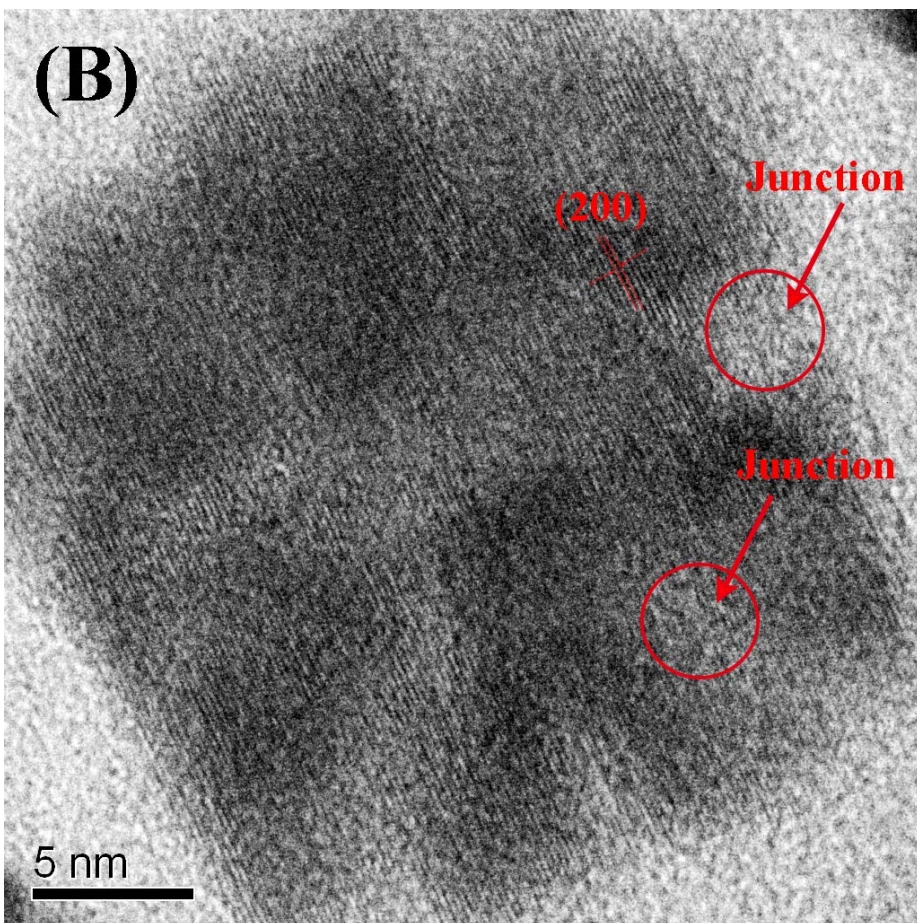
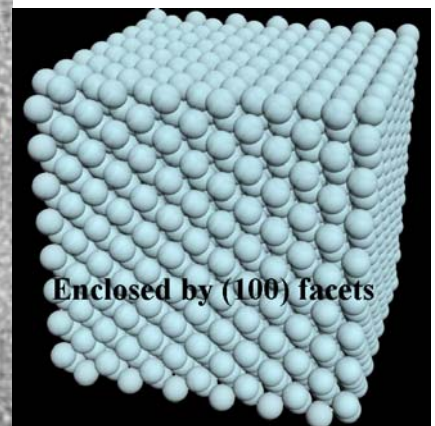
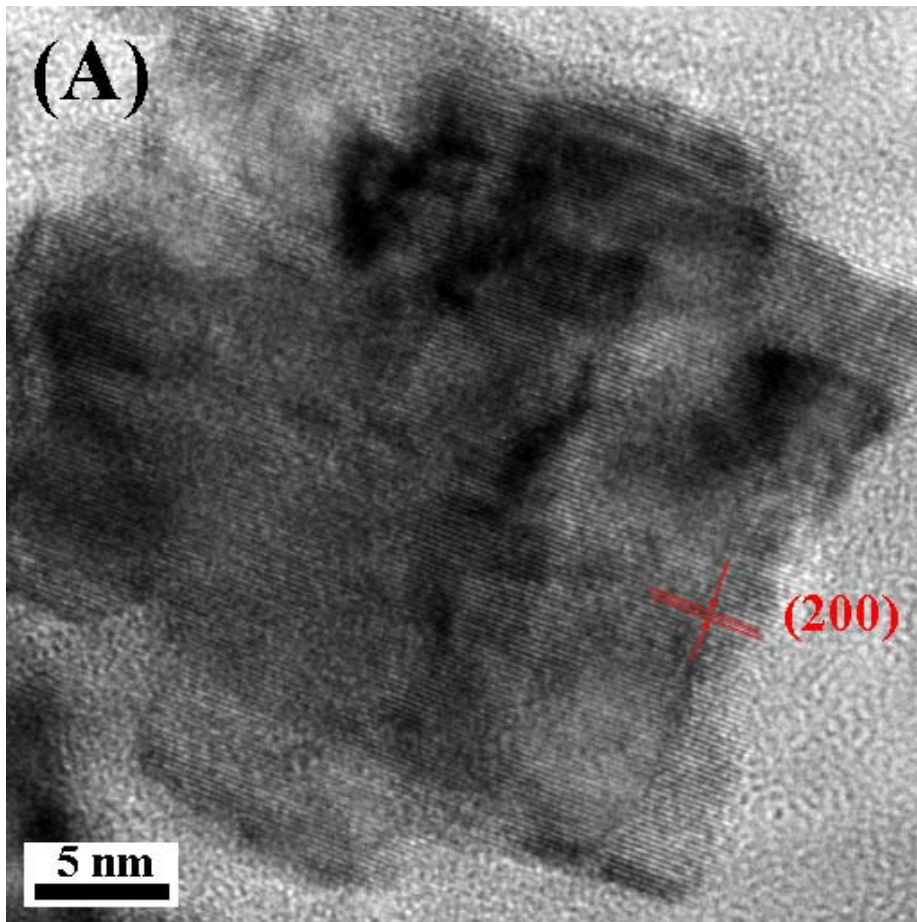


Fig. S3 HAAD-STEM-EDS element line scan profile of single Pt₅₀Pd₅₀ CS from a to b as marked in the HAAD-STEM Inset.



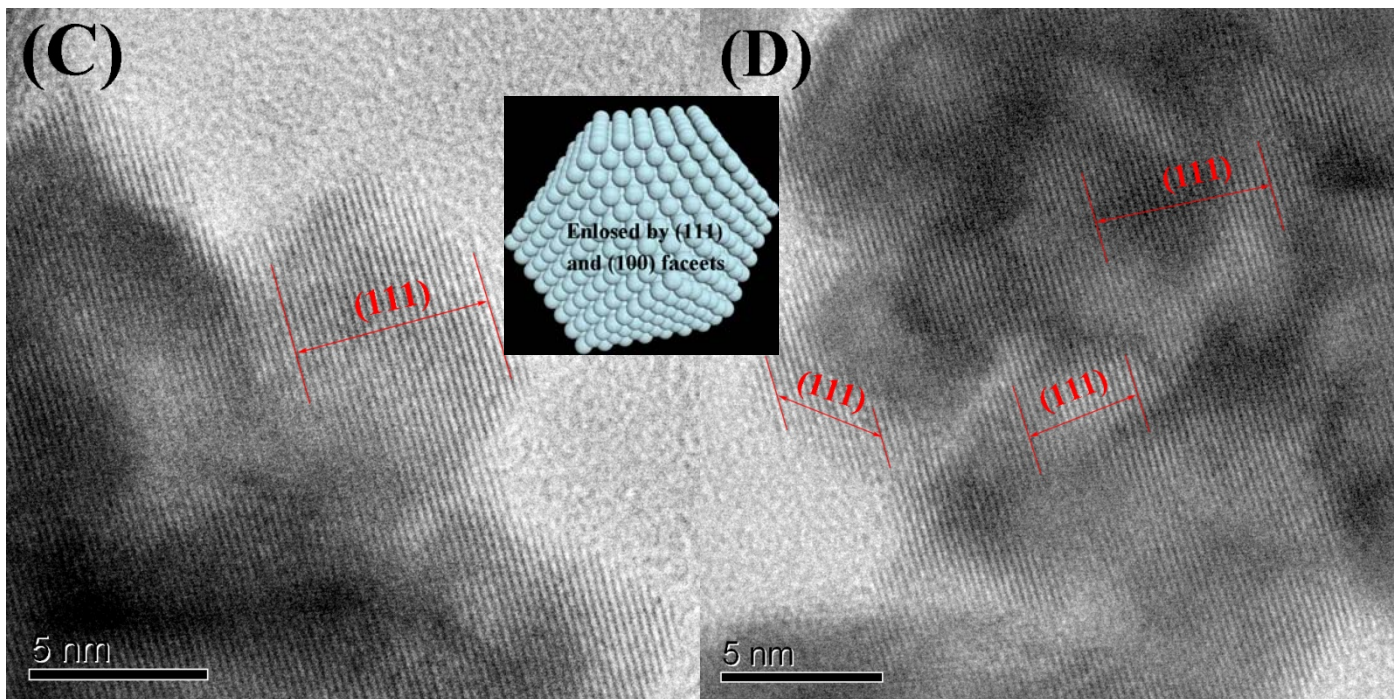
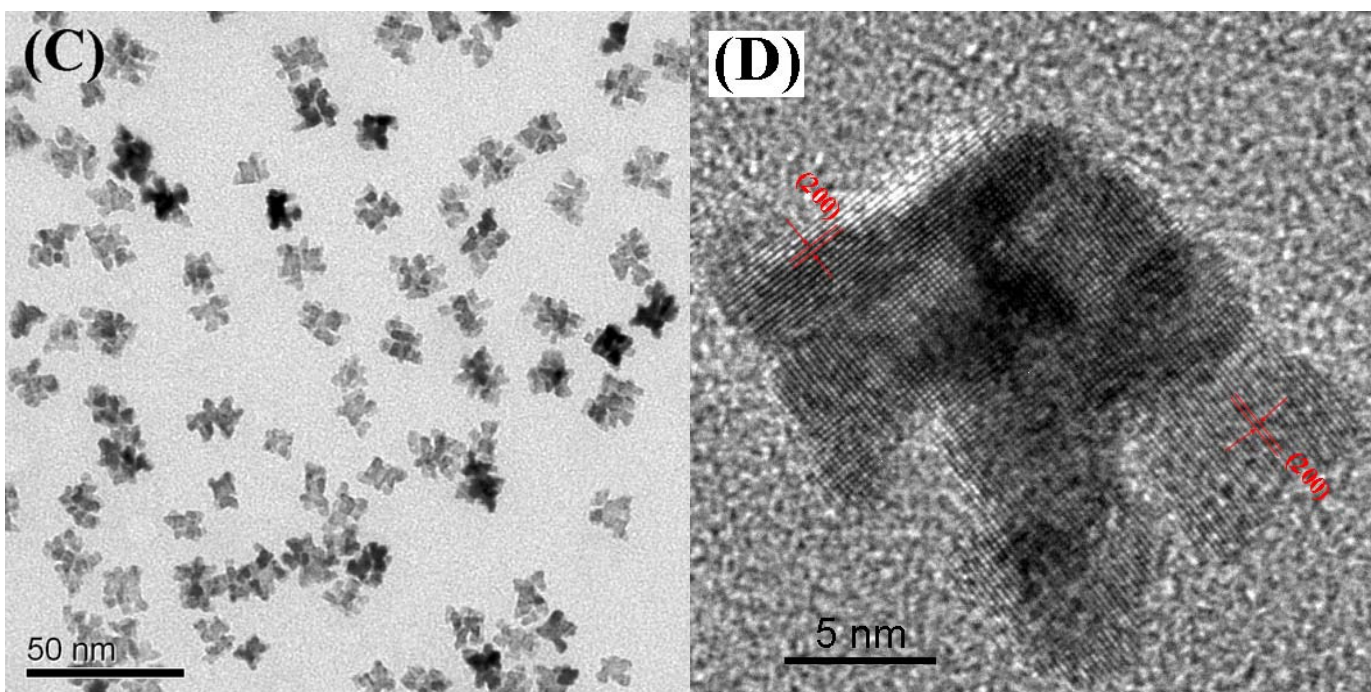
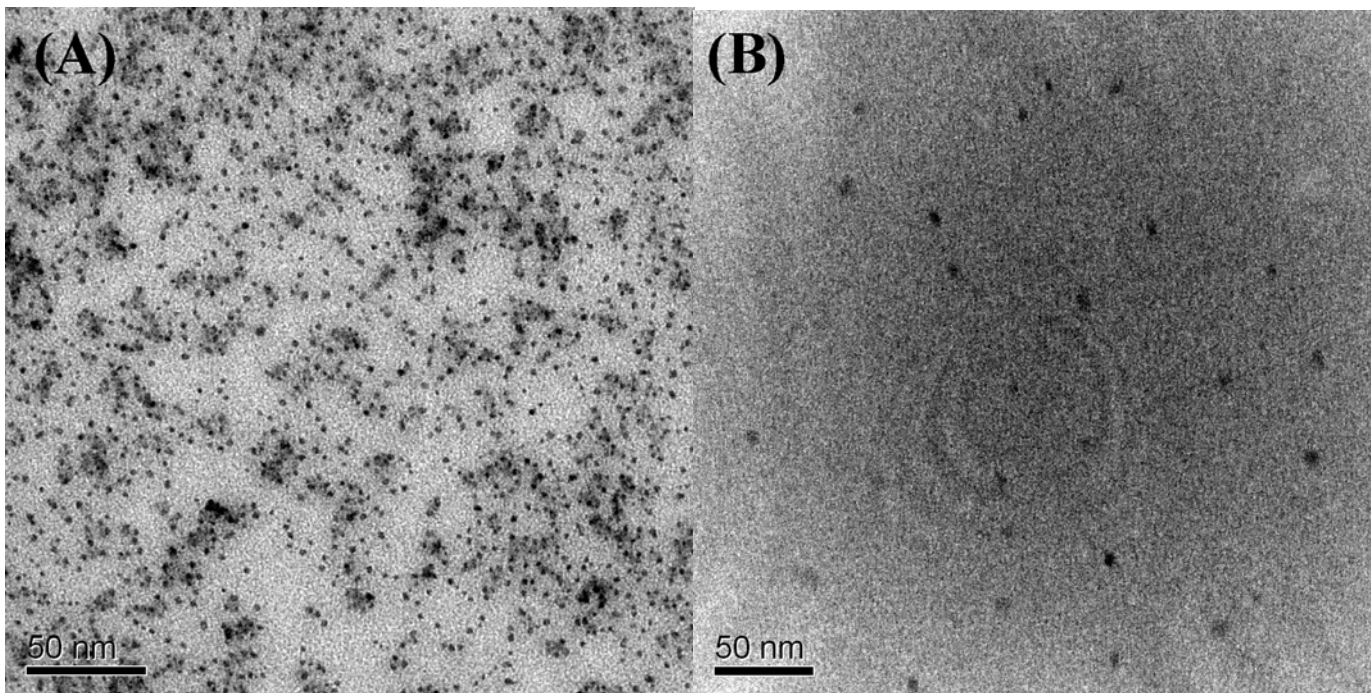
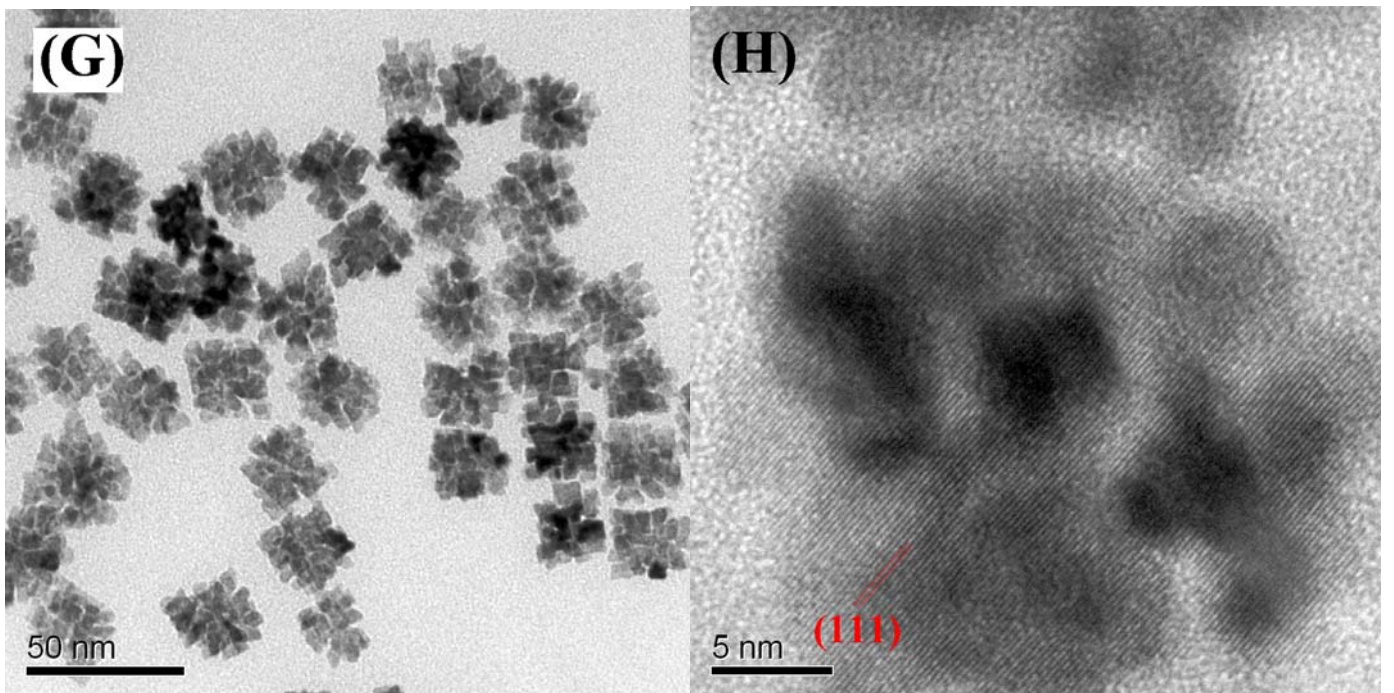
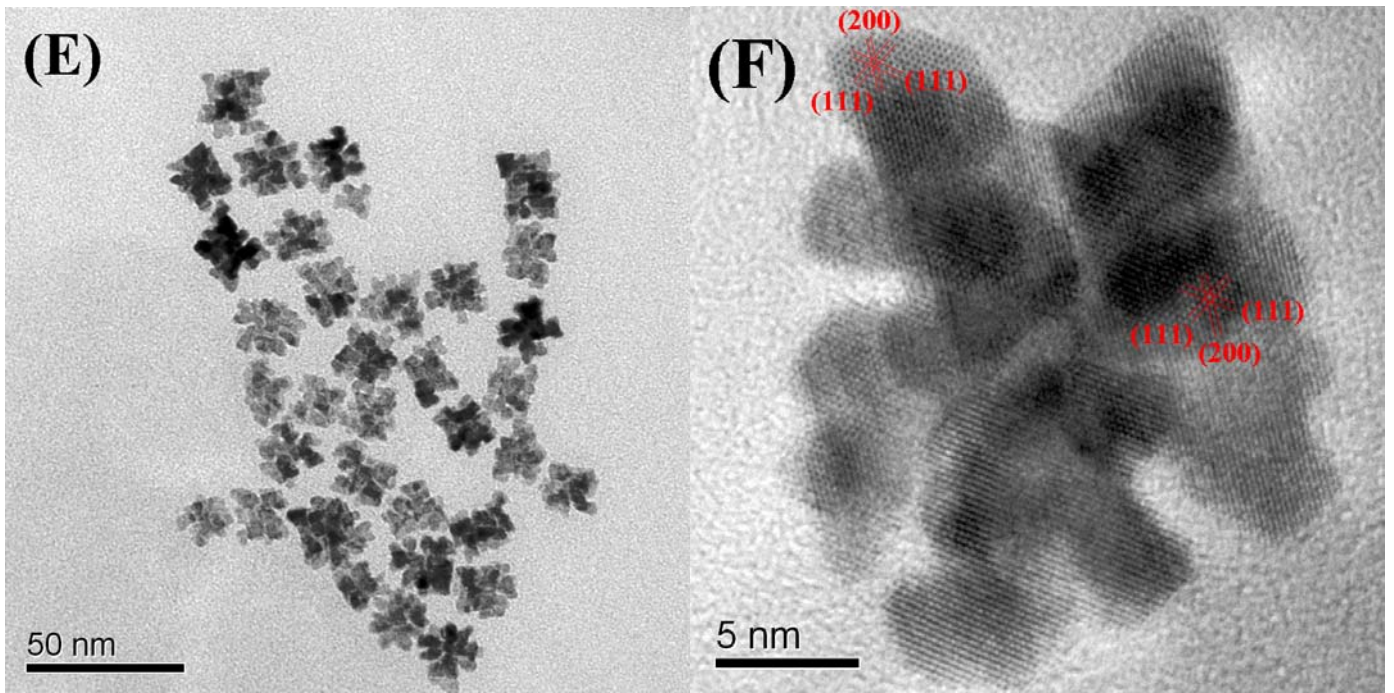


Fig. S4 HRTEM images of Pt₅₀Pd₅₀ CSs.



(To be continued)



(To be continued)

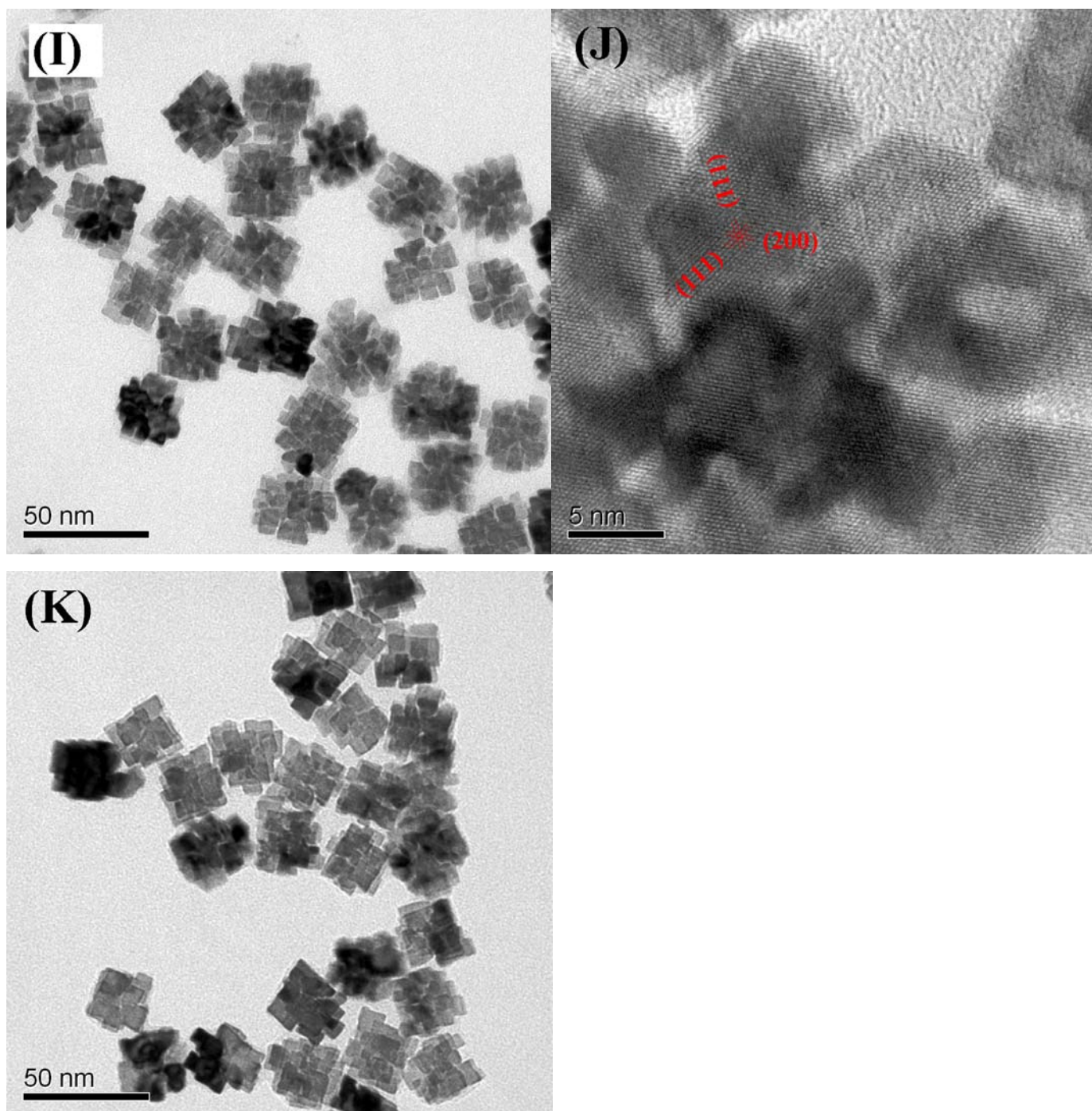


Fig. S5 TEM images of intermediates at different reaction stages: (A) 2 min, (B) 8 min, (C and D) 10 min, (E and F) 12 min, (G and H) 16 min, (I and J) 27 min, and (K) 45 min. The lattice fringes extend to the same direction and lattice fringe spacing is measured as ~ 0.23 nm and ~ 0.20 nm, corresponding to the reflections of (111) and (200) facets, respectively, as marked in Fig. S5D, F, H and J, indicating that $\text{Pt}_{50}\text{Pd}_{50}$ CSs experience a burst orientation attachment at 10 min and then a oriented growth.



0 min 2 min 6 min 60 min

Fig. S6 Digital images of the color of PtCl_6^{2-} and PdCl_4^{2-} solution at different reaction time (at 2 min, part of PdCl_4^{2-} have been converted into Pd^0 , which shows a brown color, whereas PtCl_6^{2-} solution still remains the similar color to that at the beginning (0 min)).

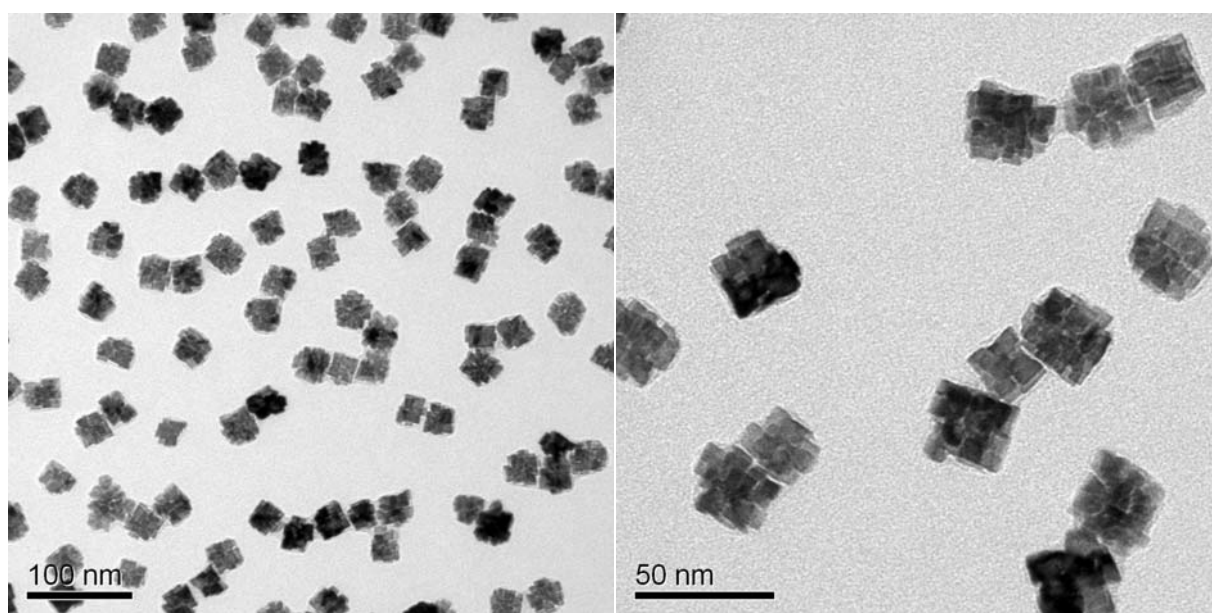


Fig. S7 TEM images of $\text{Pt}_{50}\text{Pd}_{50}$ CSs after 90-min reaction time.

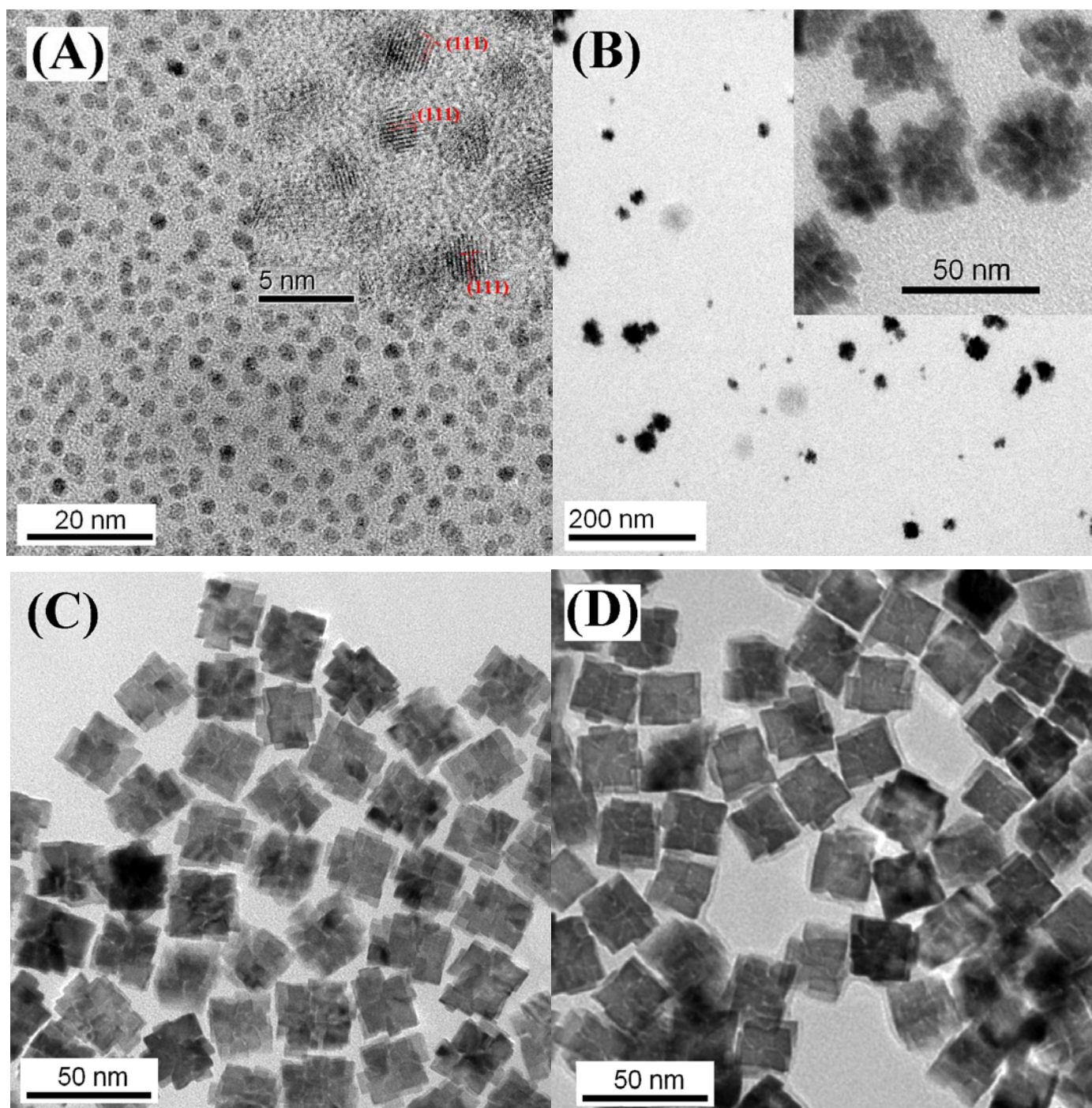


Fig. S8 TEM images of Pt₅₀Pd₅₀ nanostructures with different amount of KI: (A) without KI, (B) 50 μ L, (C) 170 μ L, and (D) 210 μ L. The standard synthetic protocol (see experimental section) contains 110 μ L of 5 M KI. Inset is HRTEM image of Pt₅₀Pd₅₀ with 50 μ L of KI.

Without I^- ions, as-prepared NPs are \sim 3-nm NPs with a Pt:Pd atomic ratio of 49.71:50.29 (Fig. S8A). HRTEM image reveals that these NPs are single crystals growing along the (111) orientation (Inset in Fig. S8A), implying that co-reduction of Pt^{IV} and Pd^{II} dominated the growth of PtPd alloy without the participation of the galvanic replacement. When 50 μ L of 5

M KI stock solution was added, the flower-like PtPd alloy aggregates with different sizes were obtained (Fig. S8B), indicating that the addition of Γ^- suppressed the reduction of Pt^{IV} and induced the occurring of the galvanic replacement between Pd^0 and Pt^{IV} . However, a small quantity of Γ^- ions could not effectively protect (100) facets so that the galvanic replacement took place everywhere on NP surfaces and flower-like $\text{Pt}_{50}\text{Pd}_{50}$ alloy aggregates instead of $\text{Pt}_{50}\text{Pd}_{50}$ CSs were produced. $\text{Pt}_{50}\text{Pd}_{50}$ CSs could be prepared when the added amount of KI solution reached to 110 μL (Fig. 1A). Continuously increasing the KI amount gradually resulted in the formation of straight sides (Fig. S8C and D) due to the full protection for (100) facets. On the other hand, the increase of KI amount also enhanced the capability of particles against the galvanic replacement so that the final products only contained a few small cavities or narrow gaps (Fig. S8D).

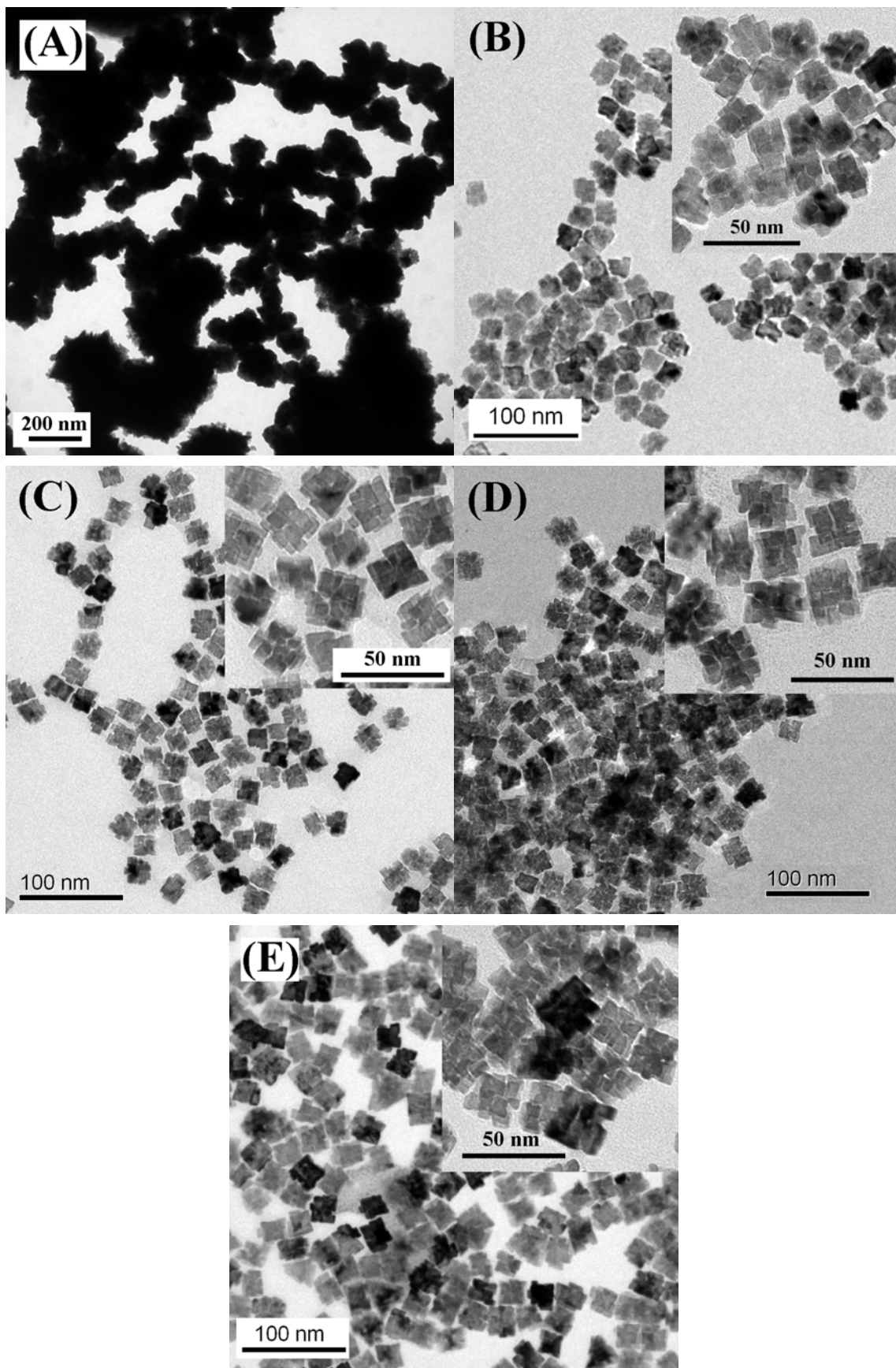


Fig. S9 TEM images of Pt₅₀Pd₅₀ nanostructures with different amount of PVP: (A) without PVP, (B) 21 mg, (C) 80 mg, (D) 320 mg, and (E) 800 mg.

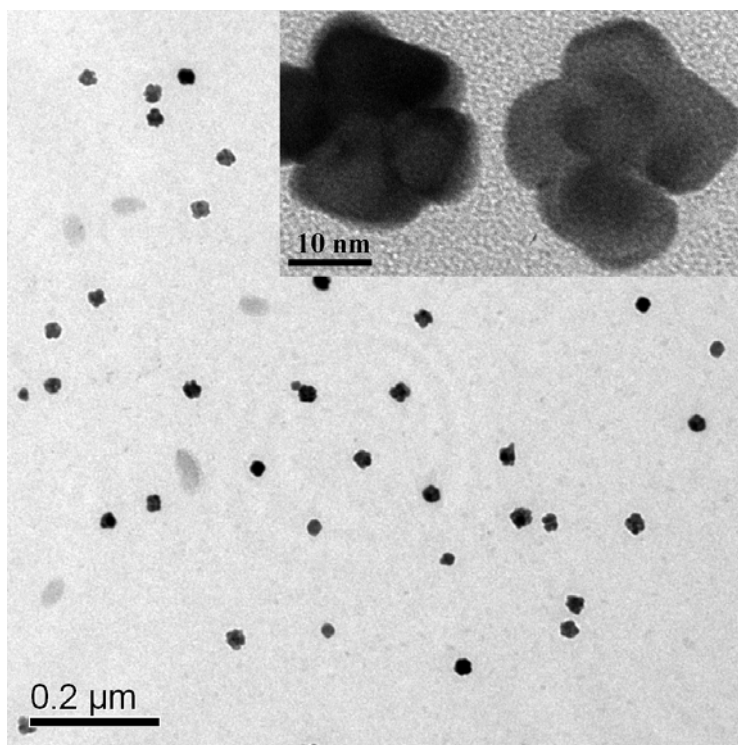
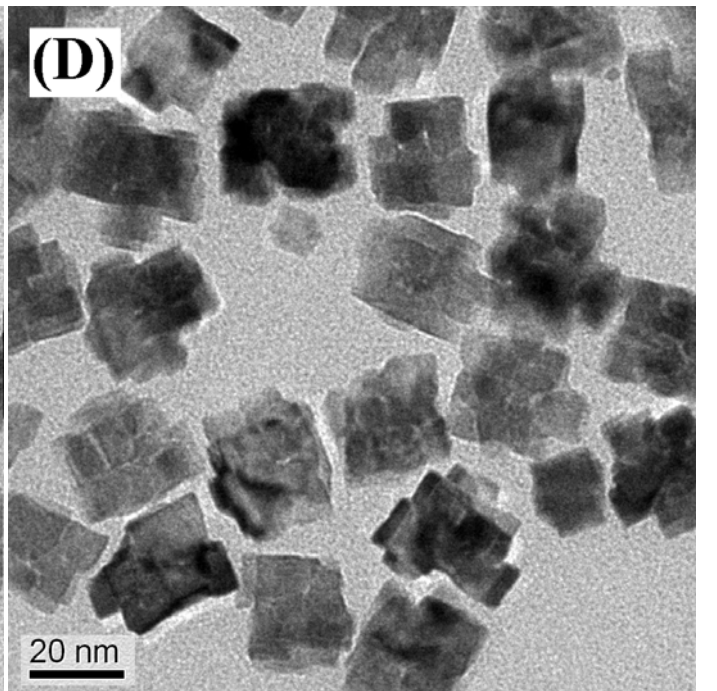
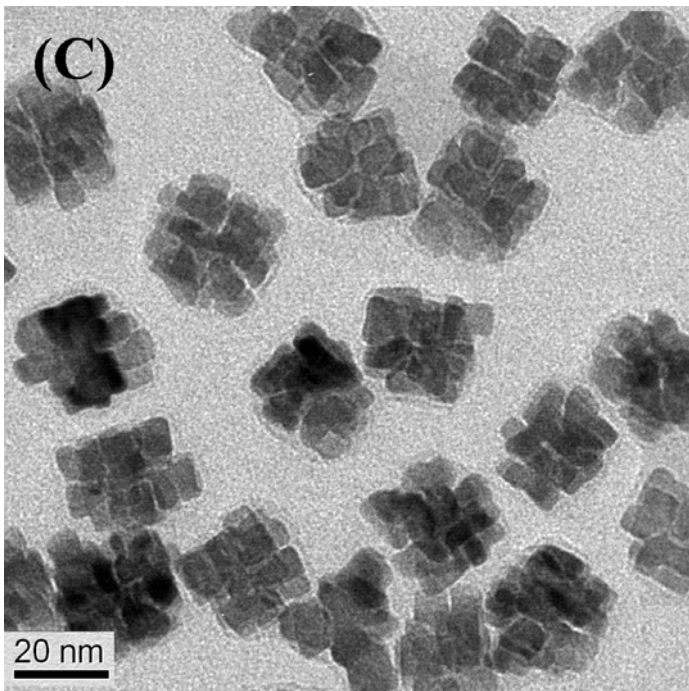
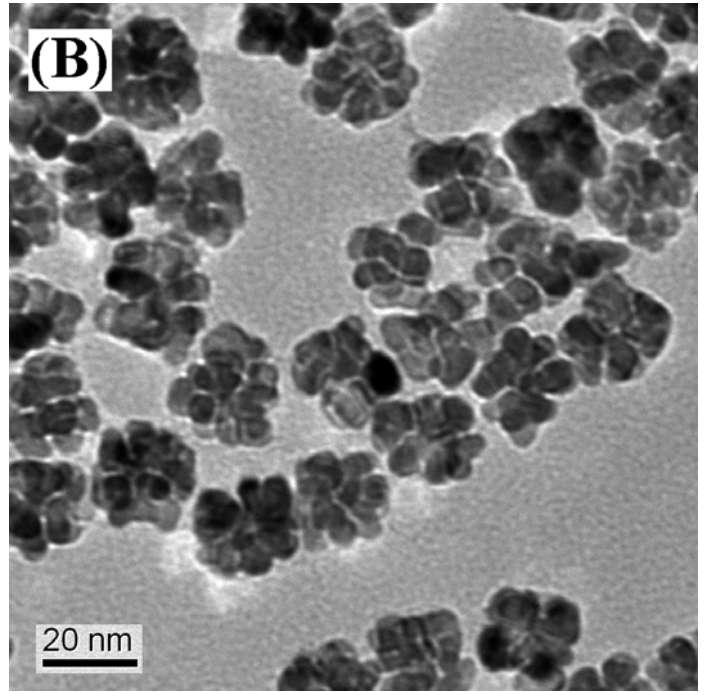
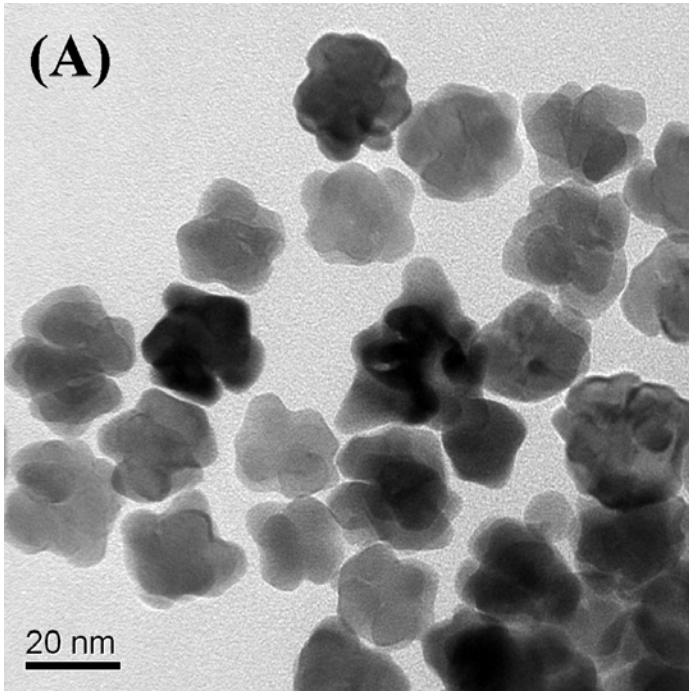


Fig. S10 TEM image of Pt₅₀Pd₅₀ nanoparticles without EG.



(To be continued)

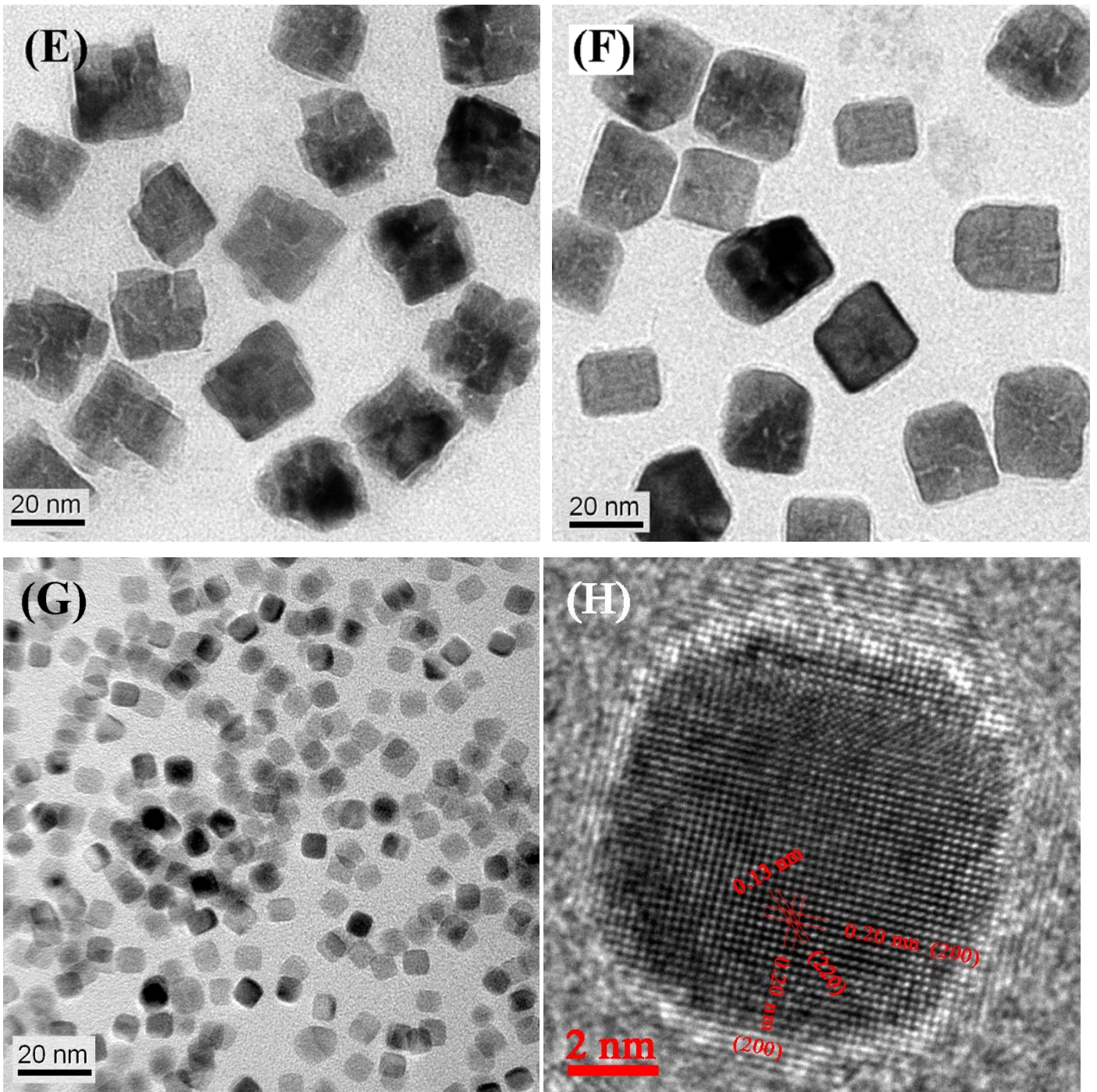


Fig. S11 TEM images of Pt (A), Pt₇₁Pd₂₉ (B), Pt₆₀Pd₄₀ (C), Pt₄₀Pd₆₀ (D), Pt₃₂Pd₆₈ (E), Pt₂₂Pd₇₈ (F) and Pd (G), and HRTEM of Pd (H).

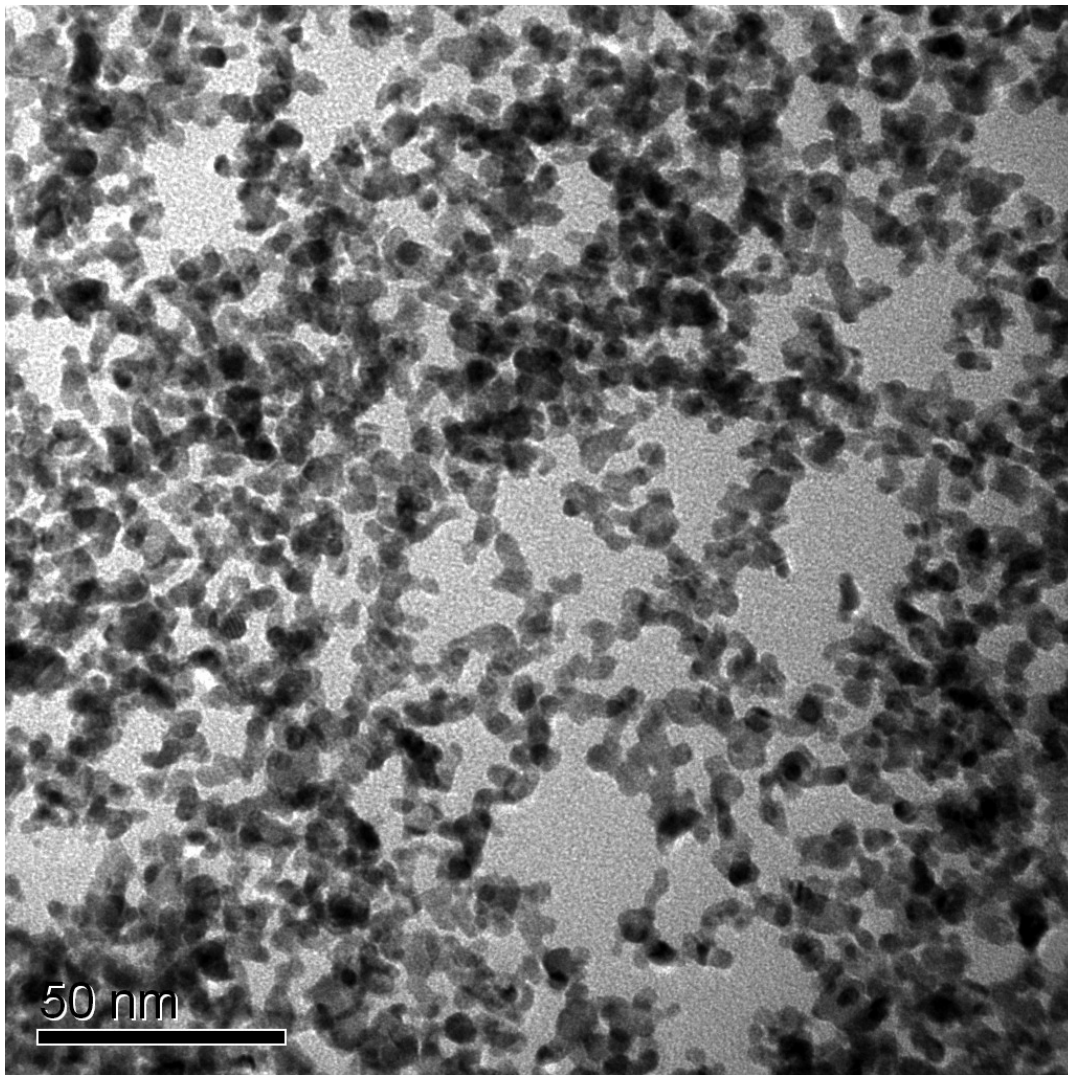


Fig. S12 TEM images of Pt₅₀Pd₅₀ particles produced at pH = 8.

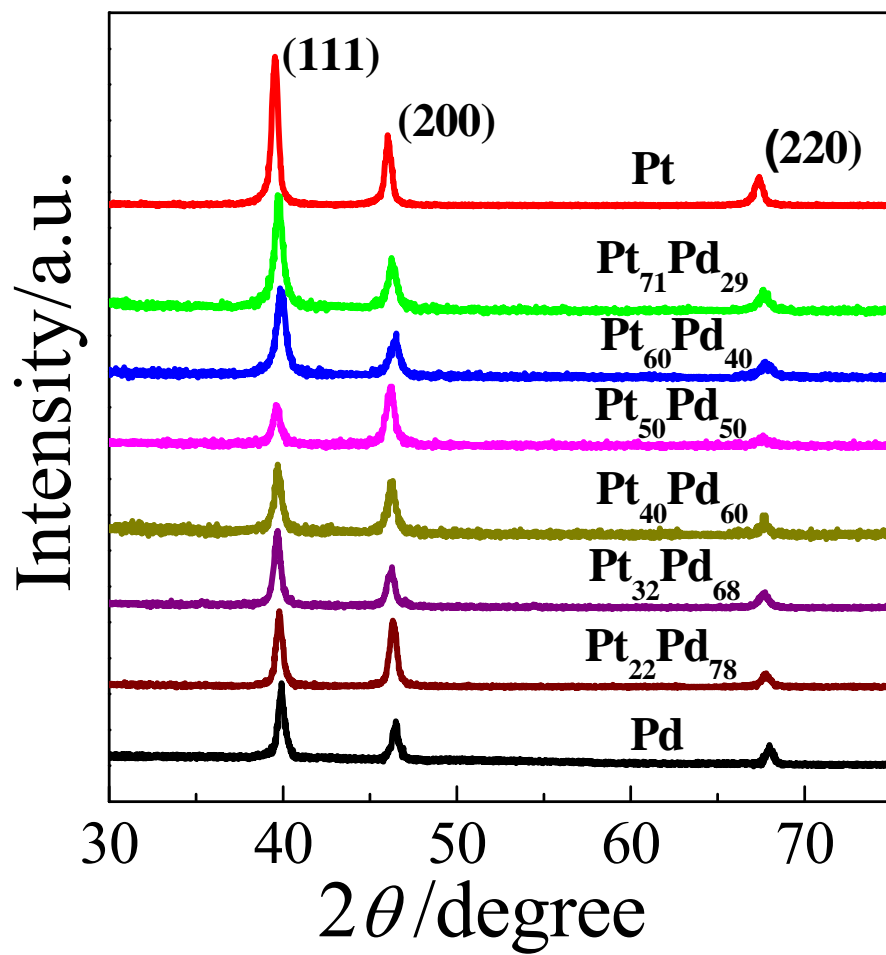


Fig. S13 XRD patterns of Pt, Pt₇₁Pd₂₉, Pt₆₀Pd₄₀, Pt₅₀Pd₅₀, Pt₄₀Pd₆₀, Pt₃₂Pd₆₈, Pt₂₂Pd₇₈ and Pd.

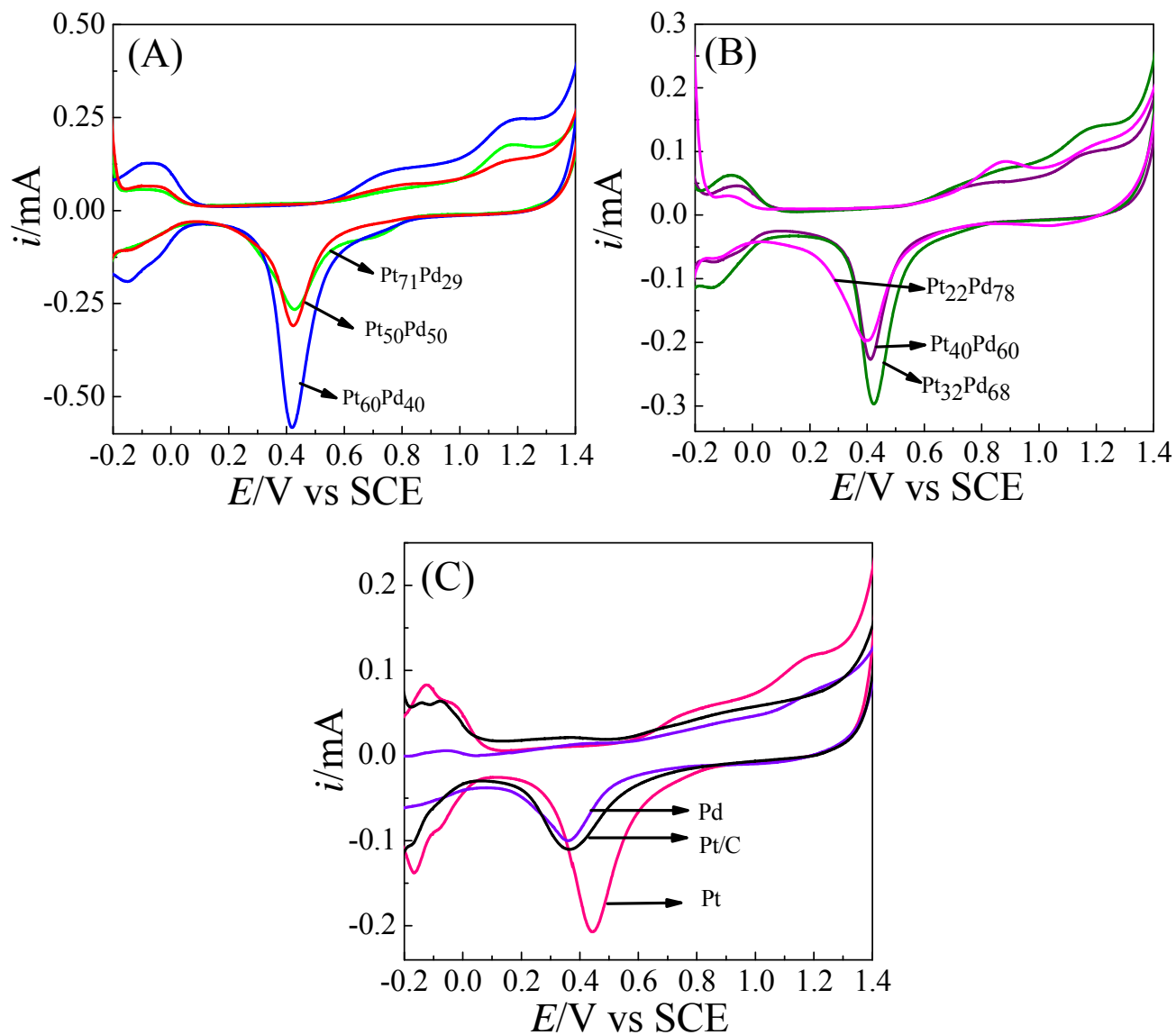


Fig. S14 Cycle voltammograms of PtPd alloy catalysts (A and B), Pt, Pd and commercial Pt/C (C) in 0.5 M H₂SO₄ at a scan rate of 50 mV·s⁻¹.

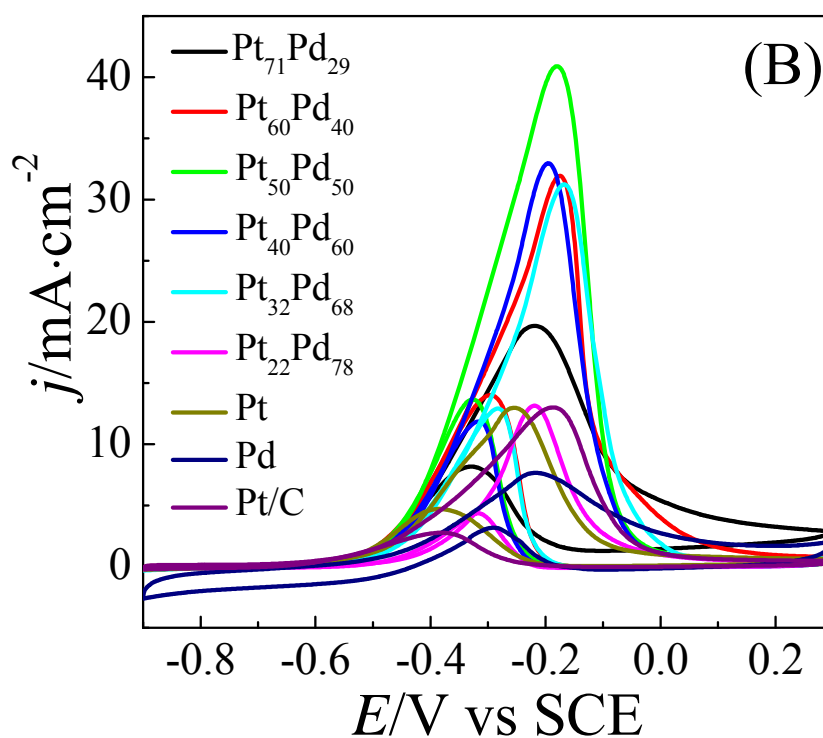
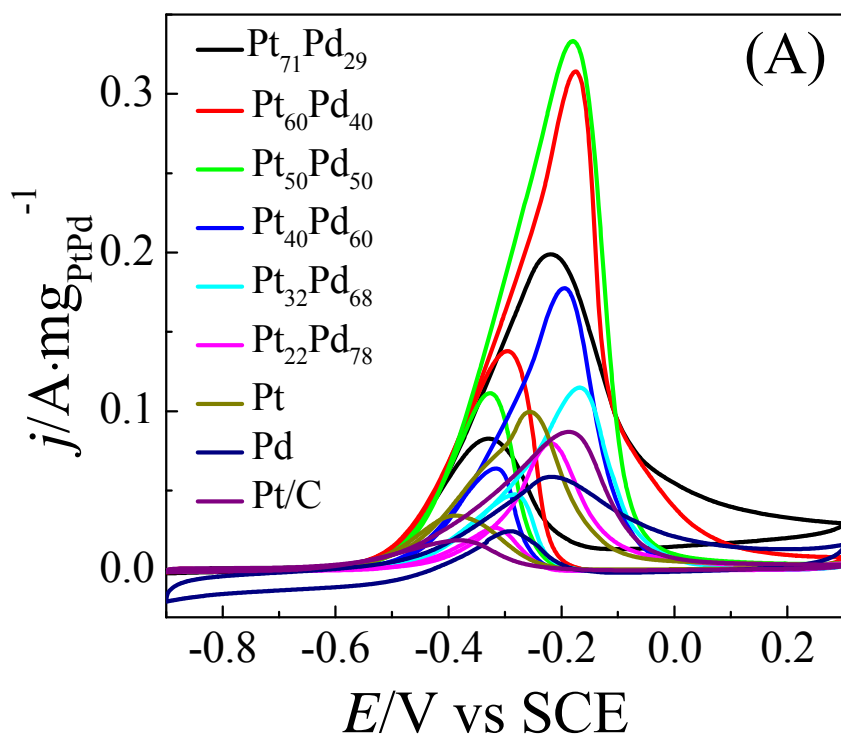


Fig. S15 Cyclic voltammograms of PtPd, pure Pt, Pd and commercial Pt/C catalysts in 1.0 M KOH containing 1.0 M methanol with scan rate of 50 mV/s: (A) the current normalized to the total mass of the corresponding catalysts and (B) the current normalized to the ECSA of the corresponding catalysts.

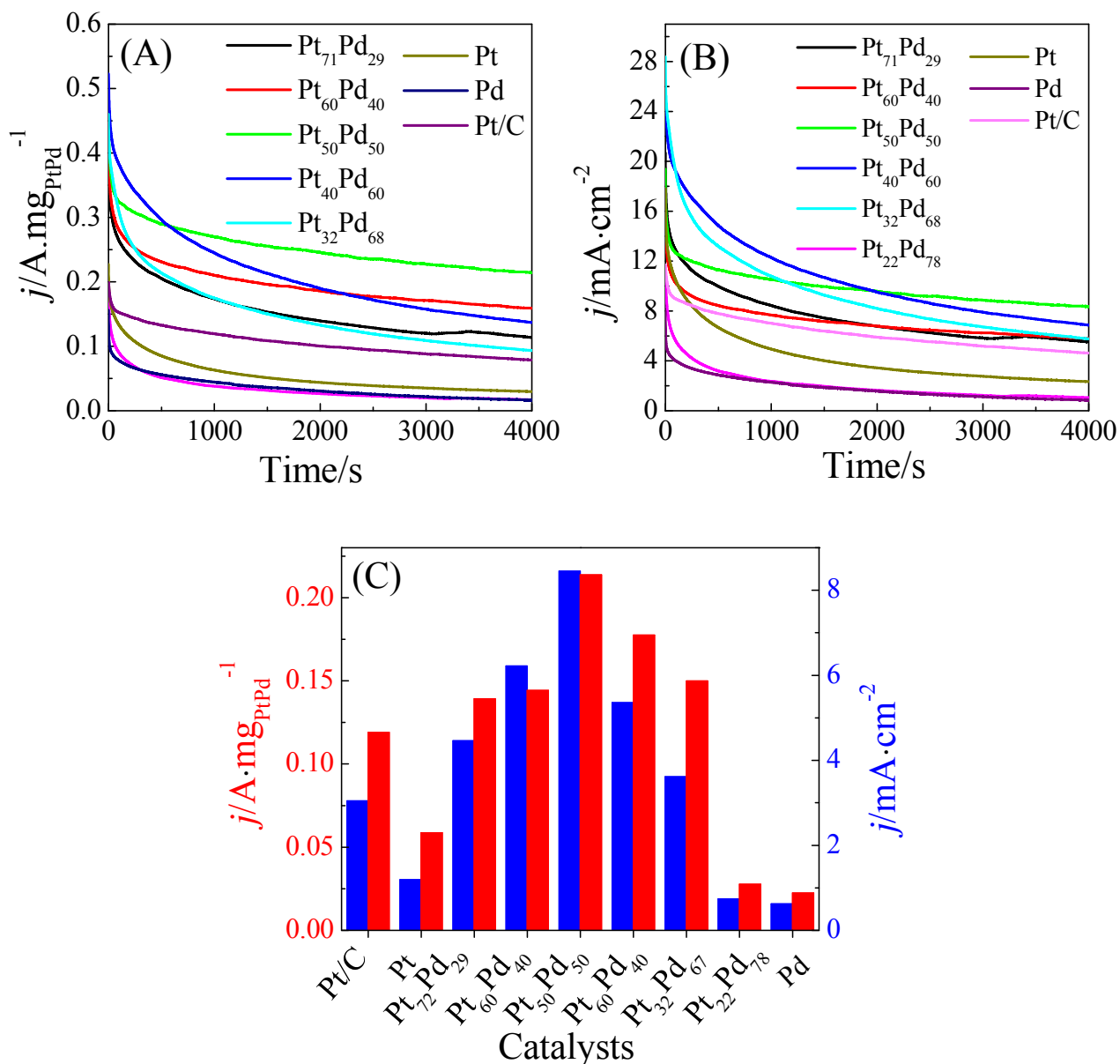


Fig. S16 (A and B) Chronoamperometric curves of PtPd alloy, pure Pt, Pd and commercial Pt/C catalysts in 1.0 M KOH containing 1.0 M methanol at -0.25 V. (C) Summary of the electrocatalytic activities of PtPd, pure Pt, Pd and commercial Pt/C catalysts at 4000 s.

Table S1 The Pt:Pd atomic ratios of the intermediates captured at different growth stages.

Time/min	Pt atomic percentage/%	Pd atomic percentage/%	Pt:Pd atomic ratio ^a
2	0	100	Pure Pd
8	65.81	34.19	66:34
10	54.35	45.65	54:46
12	52.88	47.12	53:47
16	55.43	44.57	55:44
27	53.26	46.74	53:47
45	49.37	50.63	49:51
60	49.95	50.05	50:50

^aICP-OES results.**Table S2** Feeding amount of Pt and Pd precursors and the Pt:Pd atomic ratio of the product.

Samples	Feeding amount/ 1×10^2 mmol		Feeding Pt:Pd atomic ratio	Pt:Pd atomic ratios of the product ^a
	H ₂ PtCl ₆	H ₂ PdCl ₄		
Pt	2	0	N/A	Pure Pt
Pt ₇₁ Pd ₂₉	1.40	0.60	70:30	70.90:29.10
Pt ₆₀ Pd ₄₀	1.20	0.80	60:40	60.36:39.66
Pt ₅₀ Pd ₅₀	1.00	1.00	50:50	49.95:50.05
Pt ₄₀ Pd ₆₀	0.80	1.20	40:60	40.18:59.82
Pt ₃₂ Pd ₆₈	0.60	1.40	30:70	32.28:67.72
Pt ₂₂ Pd ₇₈	0.40	1.60	20:80	21.89:78.11
Pd	0	2	N/A	Pure Pd

^aICP-OES results**Table S3** Concentration and volume of PtPd catalyst ink for preparation of catalytic electrode and the electrochemical active surface area (ECSA).

Catalysts	Concentration/mg _{metal} mL ⁻¹ ^a	The volume of catalyst ink / μ L	ECSA/m ² g ⁻¹
Pt	0.534	9.4	25.51
commercial Pt/C	0.600	8.3	34.06
Pt ₇₁ Pd ₂₉	0.475	10.5	41.16
Pt ₆₀ Pd ₄₀	0.550	9.1	54.67
Pt ₅₀ Pd ₅₀	0.598	8.4	51.36
Pt ₄₀ Pd ₆₀	0.614	8.1	39.93
Pt ₃₂ Pd ₆₈	0.521	9.6	32.47
Pt ₂₂ Pd ₇₈	0.736	6.8	37.06
Pd	0.575	8.7	12.95

^aICP-OES results

Table S4 Summary of electrocatalytic activity of Pt-, Pd- and PtPd-related catalysts towards methanol oxidation in basic solution.

Catalysts	Mass activity/mA mg ⁻¹	Specific activity/mA cm ⁻²	Reference
Pt ₇₁ Pd ₂₉	199	19.7	This study
Pt ₆₀ Pd ₄₀	313	30.1	
Pt ₅₀ Pd ₅₀	336	40.4	
Pt ₄₀ Pd ₆₀	178	32.9	
Pt ₃₂ Pd ₆₈	115	31.2	
Pt ₂₂ Pd ₇₈	80.9	13.2	
Pt ₇₄ Pd ₂₆ concave nanocubes/graphene	381	–	2
Pd ₄₅ Pt ₅₅ alloy nanowires	~2000	–	3
Pd ₁ Pt ₁ /graphene	–	7.69	4
Pt–Pd nanodendrites		120	5
Pt ₂ Pd ₁ nanogarlands/graphene	333	–	6
Dendritic PdPt alloy nanoparticles	~102	0.57	7
Pd ₅ Pt ₁ alloy nanoflowers/graphene	400	2.16	8
PdCuSn/CNTs	~400	–	9
Pt _{0.75} Pd _{0.13} Cu _{0.12} nanocrystals	–	3.47	10
Pd-TiO ₂ /C	–	23	11
Pt ₃ Ni ₁ /C	~414 (relative to Pt mass)	–	12

References

- (1) Ramirez-Aguilar, K. A.; Rowlen, K. L. *Langmuir* **1998**, *14*, 2562.
- (2) Lu, Y.; Jiang, Y.; Chen, W. *Nanoscale* **2014**, *6*, 3309.
- (3) Zhu, C.; Guo, S.; Dong, S. *Adv. Mater.* **2012**, *24*, 2326.
- (4) Ji, H.; Li, M.; Wang, Y.; Gao, F. *Electrochem. Commun.* **2012**, *24*, 17.
- (5) Lv, J.-J.; Zheng, J.-N.; Chen, L.-L.; Lin, M.; Wang, A.-J.; Chen, J.-R.; Feng, J.-J. *Electrochim. Acta* **2014**, *143*, 36.
- (6) Li, S.-S.; Zheng, J.-N.; Ma, X.; Hu, Y.-Y.; Wang, A.-J.; Chen, J.-R.; Feng, J.-J. *Nanoscale* **2014**, *6*, 5708.
- (7) Kang, S. W.; Lee, Y. W.; Park, Y.; Choi, B.-S.; Hong, J. W.; Park, K.-H.; Han, S. W. *ACS Nano* **2013**, *7*, 7945.
- (8) Wu, K.; Zhang, Q.; Sun, D.; Zhu, X.; Chen, Y.; Lu, T.; Tang, Y. *Int. J. Hydrogen Energy* **2015**, *40*, 6530.

- (9) Zhu, F.; Ma, G.; Bai, Z.; Hang, R.; Tang, B.; Zhang, Z.; Wang, X. *Journal of Power Sources* **2013**, *242*, 610.
- (10) Mao, J.; Cao, T.; Chen, Y.; Wu, Y.; Chen, C.; Peng, Q.; Wang, D.; Li, Y. *Chem. Commun.* **2015**, *51*, 15406.
- (11) Maheswari, P. S.; Pitchuman, S. *Electrochem. Commun.* **2013**, *26*, 97.
- (12) Jiang, Q.; Jiang, L.; Wang, S.; Qi, J.; Sun, G. *Catal. Commun.* **2010**, *12*, 67.